NANO LETTERS

Letter

pubs.acs.org/NanoLett

Graphene Plasmon Enhanced Vibrational Sensing of Surface-Adsorbed Layers

Yilei Li,[†,‡] Hugen Yan,[†] Damon B. Farmer,[†] Xiang Meng,[§,∥] Wenjuan Zhu,[†] Richard M. Osgood,[§,∥] Tony F. Heinz,[‡,§] and Phaedon Avouris*[,†]

[†]IBM T. J. Watson Research Center, Yorktown Heights, New York 10598, United States

[‡]Department of Physics, Columbia University, New York, New York 10027, United States

[§]Department of Electrical Engineering, Columbia University, New York, New York 10027, United States

[∥]Department of Applied Physics, Columbia University, New York, New York 10027, United States

Supporting Information

ABSTRACT: We characterize the influence of graphene nanoribbon plasmon excitation on the vibrational spectra of surface-absorbed polymers. As the detuning between the graphene plasmon frequency and a vibrational frequency of the polymer decreases, the vibrational peak intensity first increases and is then transformed into a region of narrow optical transparency as the frequencies overlap. Examples of this are provided by the carbonyl vibration in thin films of poly(methyl methacrylate) and polyvinylpyrrolidone. The signal depth of the plasmon-induced transparency is found to be 5 times larger than that of light attenuated by the carbonyl vibration alone. The plasmon-vibrational mode coupling and the resulting fields are analyzed using both a phenomenological model of electromagnetically coupled oscillators and finite-difference time-domain simulations. It is shown that this coupling and the resulting absorption enhancement can be understood in terms of near-field electromagnetic interactions.

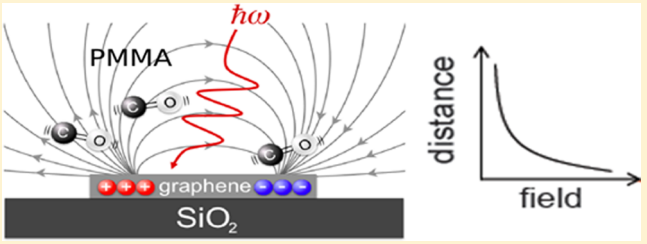

KEYWORDS: *Graphene, plasmons, polymers, vibrations, enhancement, induced transparency, infrared spectroscopy*

Graphene is a single sheet of carbon atoms arranged in a honeycomb lattice.[1−3] By patterning graphene into nanoribbons, propagating electromagnetic waves in free space can be directly coupled to bound collective charge oscillations, that is, localized plasmons.[4] Unlike in metals, the charge density in graphene can be easily modified by electrostatic gating or chemical doping, resulting in tunable plasmon resonances.[5,6] Strong light confinement and frequency tunability are two important characteristics of graphene plasmons, which make them good candidates for the enhancement of photon fields in the mid-infrared to terahertz regions of the spectrum.[7] It has already been shown that plasmon resonances in graphene can couple strongly to substrate polar phonons[8,9] and also to the intrinsic IR-active phonons of bilayer graphene.[10] A closely related, but yet unexplored problem is the interaction of plasmons in graphene with the extrinsic vibrational modes in adsorbed species. Indeed, the possibility of near-field enhancement of light-matter interactions by graphene plasmons has been predicted.[7,11] However, an experimental demonstration of such a phenomenon is still lacking. The interaction between plasmons in noble metal nanoparticles and vibrational modes in molecules has long been used as an ultrasensitive probe for sensing small molecular concentrations,[12−15] a fact that also motivates the current study.

In unpatterned graphene, the electromagnetic boundary conditions and Drude-like conductivity[16] determines the plasmon frequency, which scales with the charge density (n) and the plasmon wave vector ($\mathbf{q}$) as $\omega \propto n^{1/4}$ and $\omega \propto \mathbf{q}^{1/2}$, respectively.[17,18] In graphene nanoribbons and other forms of nanostructures, localized plasmons can be directly excited by incident light with zero in-plane momentum, and analogous dispersion relations can be obtained in the quasi-static limit,[4] which is appropriate for structures much narrower than the incident light wavelength. These graphene plasmons have resonance frequencies which, depending on their size and doping, lie in the infrared or far-infrared range of the spectrum.[9,19] Thus, the use of nanoribbons, or other forms of patterned graphene, allows for the efficient and selective coupling of infrared light to surface plasmon modes. In this work, we use infrared transmission spectroscopy to study the interaction of graphene plasmons with vibrational modes in surface-adsorbed thin polymer films. Poly(methyl methacrylate) (PMMA) and poly(vinylpyrrolidone) (PVP) are used as the adsorbates in these experiments. Both polymers contain carbonyl (C═O) groups with vibrational frequencies around 1700 cm^{-1}, but due to their different molecular structures, the exact frequencies are slightly different.

Received: December 30, 2013
Revised: February 10, 2014
Published: February 14, 2014

The structure of the fabricated samples is shown in Figure 1a. The nanoribbon array is defined by electron beam lithography

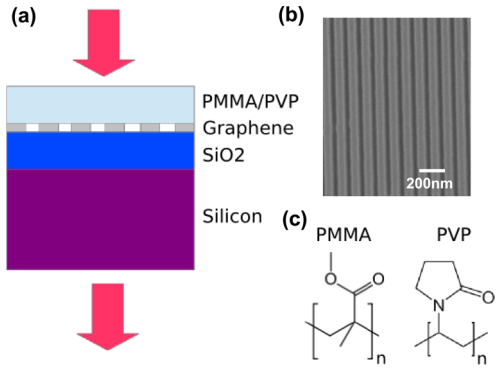

Figure 1. (a) Experimental arrangement. Our measurement is conducted in the light transmission configuration. The sample is composed of a thin layer of PMMA or PVP, a graphene nanoribbon (GNR) array, and a 280 nm thick SiO_2 layer on top of a bulk Si substrate. (b) SEM image of graphene nanoribbons. (c) PMMA and PVP both contain the carbonyl double-bond (C═O), whose stretching mode has a vibrational frequency around 1700 cm^{-1}.

and etching of graphene grown by chemical vapor deposition (CVD) (Figure 1b). Highly resistive silicon with 280 nm thick surface oxide is used as the substrate that allows light transmission in the mid-infrared range. PMMA layers are spin-coated onto the nanoribbon-covered substrates. The thicknesses of these layers are determined by ellipsometry and controlled using PMMA solutions of different concentrations. Samples with PVP are also prepared by spin-coating, but the thickness of this film is further decreased by washing in copious amounts of water. This dissolves the portion of the polymer that is not in direct contact with the sample surface, leaving a PVP residue that is only 2−3 nm thick, as determined by height and phase-contrast AFM. The carbonyl-containing structures of PMMA and PVP are shown in Figure 1c. IR spectra of these samples are collected in the transmission configuration using an IR microscope coupled to an FTIR spectrometer (Thermo Scientific Nicolet Continuum Infrared Microscope and Nicolet 8700 FTIR spectrometer). The attenuation of the transmission is defined as $A = 1 - T/T_0$ where T is the transmission spectrum with graphene nanoribbons and T_0 is the transmission spectrum of the same system without graphene nanoribbons.

Figure 2a shows the attenuation spectra of graphene nanoribbons (90 nm wide) with an 8 nm thick PMMA overlayer for light in resonance with the nanoribbon plasmon polarized perpendicular and parallel to the ribbons. Here, the polarization dependence of plasmon attenuation is utilized, that is, plasmons are excited in the nanoribbons when the polarization is perpendicular to the ribbon length, but not when the polarization is parallel.[9,20] A sharp transparency valley in the attenuation spectra of plasmon resonance is observed at the frequency of the stretching mode of the carbonyl double bond. The depth of this valley is 0.63%, while without the graphene the height of the PMMA film attenuation feature is only 0.25%. Taking into account the filling factor of the graphene ribbons, this corresponds to a 5-fold increase in the vibrational absorption sensitivity. This plasmon-induced transparency (PIT) can be understood as a special case of coherent destructive interference between two mutually coupled excitations with very different couplings to an external driving field. Analogous phenomena have been observed in optical (three level atoms),[21] mechanical,[22] and electrical systems.[23] In our PIT case, one of these excitations is the plasmon which is strongly coupled to the radiation field (with a femtosecond lifetime), while the carbonyl vibration (picosecond lifetime) is more weakly coupled.[10,24]

Enhancement of the vibrational absorption is observed even when there is only a partial overlap between the plasmon and vibrational frequencies. The localized plasmon frequency depends on the ribbon width W, $\omega \propto 1/\sqrt{W}$, so by using graphene nanoribbons of different widths, the plasmon resonance can be translated across the vibrational mode resonance. Figure 2b shows the attenuation spectra of three graphene nanoribbon arrays (110, 120, and 130 nm width) coated with 8 nm of PMMA. The plasmon attenuation peak intensity is normalized, and the vibration appears as a peak at the high-energy side of the plasmon. We observe that the vibrational attenuation increases as the detuning between plasmon and vibrational frequency decreases ($\Delta I \sim 1/\Delta f$),

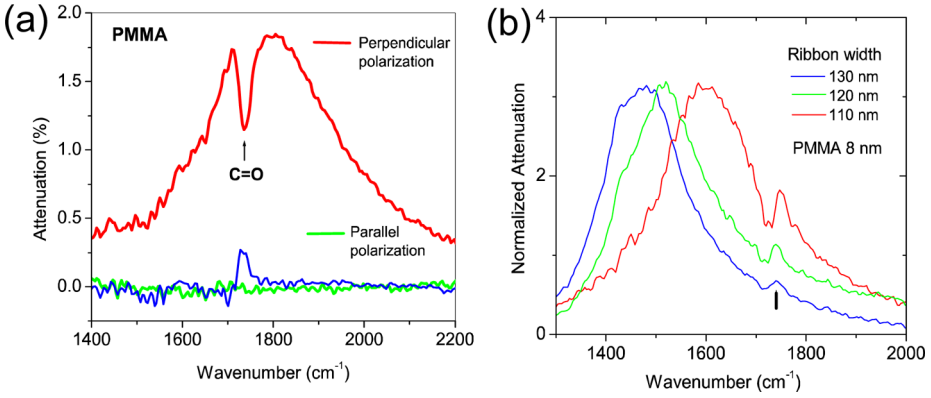

Figure 2. (a) Attenuation spectra for light in resonance with the graphene plasmon polarized perpendicular (red line) and parallel (green line) to the graphene nanoribbons. An 8 nm thick PMMA is spin-coated onto 90 nm graphene nanoribbons. Surface plasmons are excited in the perpendicular polarization case, but not excited in the parallel polarization case. The attenuation spectrum of an 8 nm thick PMMA layer (without nanoribbons) is shown as the blue line. (b) Attenuation spectra of three graphene nanoribbon arrays (110, 120, and 130 nm width) coated with 8 nm of PMMA. The plasmon attenuation peak intensity is normalized, and the vibration appears as a peak at the high-energy side of the plasmon. The plasmon and vibrational excitations overlap only partially.

dx.doi.org/10.1021/nl404824w | Nano Lett. 2014, 14, 1573−1577

clearly demonstrating that the enhancement is a resonance effect.

To understand the origin of the IR absorption enhancement, we performed finite-difference time-domain (FDTD) simulations in which the device structure is taken to be the same as in Figure 1a. The plasmon is excited in the nanoribbon by a plane wave whose frequency is in resonance with the plasmon, and periodic boundary conditions are used to simulate the array of nanoribbons. The conductivity of graphene is assumed to follow a Drude form. Furthermore, the DC conductivity and the scattering rate in the Drude form determine the resonance frequency and the width of the plasmon peaks, respectively. In general, the effectiveness of the plasmonic effects of a system is quantified by the quality factor Q given by $Q = -Re\varepsilon/Im\varepsilon$, where ε is the complex dielectric function of the plasmonic material. The local optical field intensity enhancement responsible for the increase in absorption is proportional to Q^2 (in Raman scattering $\propto Q^4$). It is therefore clear that the quality factor of the plasmonic resonance plays a very important role in the field enhancement and will be a function of frequency as different decay pathways (damping) may be involved at different energies.[9,17] In Figure 3 we show results

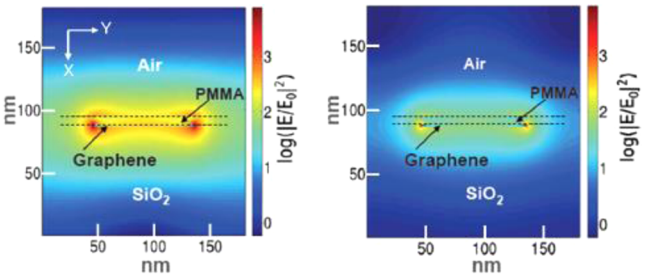

Figure 3. Spatial map of the enhancement of electric field intensity near a graphene nanoribbon both perpendicularly to the surface of the nanoribbon (X) and across the nanoribbon (Y). Finite-difference time-domain (FDTD) simulations of the field enhancement in the vicinity of nanoribbons for two values of plasmon damping, $\gamma = 50$ cm^{-1} (left) and $\gamma = 250$ cm^{-1} (right).

for two different plasmon widths (damping rates) $\gamma = 50$ cm^{-1} and $\gamma = 250$ cm^{-1}. Further details of this simulation are given in the Supporting Information. The enhancement in the field intensity is expressed by taking the ratio of the electric field intensities with and without the nanoribbons at each spatial point, $|E^2/E_0^2|$. As can be seen from the color-coded Figure 3, large enhancements in the field intensity can be generated (more than 3 orders of magnitude) near the edges of the nanoribbon and that the field enhancement decays exponentially away from both the edges and the graphene surface. This enhancement in the local electric field is the source of the observed enhancement in the interaction between light and the carbonyl vibration in the polymer film. This enhancement can be potentially further increased through improved graphene sample quality (reduced plasmon damping), and by the use of stacked graphene layers.[19] These optimization procedures deserve further work but are beyond the scope of the present study.

Figure 4 illustrates the variation of the vibrational spectrum as a function of the detuning between the plasmon and the vibrational excitation. To understand qualitatively the variation in intensity and line shape, we model the system using a pair of coupled electrical dipole oscillators.[23] In this model, the

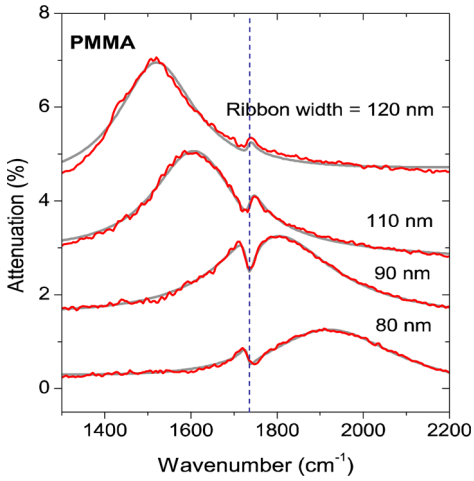

Figure 4. Graphene plasmon extinction spectra for different graphene nanoribbon widths. The changes in intensity, line shape, and the development of a transmission transparency near the 1750 cm^{-1} C=O vibration are due to the interaction of the graphene plasmon and the molecular vibration in PMMA. The gray lines are phenomenological fits using the coupled electrical dipole oscillator model (see text).

plasmon in graphene and carbonyl vibration in the polymer are represented by two dipole oscillators that are coupled to one another. Within the quasi-static approximation, the relations between the physical parameters in this model are summarized in the following coupled differential equations:

$$\ddot{x}_1^{\,2} + \gamma_1\dot{x}_1 + \omega_1^{\,2}x_1 = A_1e^{i\omega t} - C_{12}x_2 \quad (1a)$$

$$\ddot{x}_2^{\,2} + \gamma_2\dot{x}_2 + \omega_2^{\,2}x_2 = -C_{21}x_1 \quad (1b)$$

Here, x_1 and x_2 denote the electric polarizations corresponding to the graphene plasmon and the carbonyl vibrational mode response to the plasmon, γ_1 and γ_2 denote the decay rates of the graphene plasmon and the vibrational mode, ω_1 and ω_2 are their respective resonant frequencies, C_{12} and C_{21} are the coupling constants between the two dipoles, and A_1 is proportional to the amplitude of the driving electric field. The total transmission attenuation of a thin sheet, which is proportional to the real part of the conductivity,[25] can then be obtained. The vibrational frequency of the carbonyl group ω_2 is fixed, and the other parameters are varied. For more details, see the Supporting Information. As shown in Figure 4 (gray line), this phenomenological model successfully describes the observed evolution of the spectrum, from nearly symmetric resonances to asymmetric peaks (Fano line shape) and the transmission transparency.

For practical applications, it is important to know the effective range of the enhancement of the optical fields by the graphene plasmons. The FDTD simulations indicate that this enhancement length (enhancement drops to 1/e of its maximum) is quite short (see Figure 3). This issue can also be experimentally addressed by varying the thickness of the polymer overlayer. Attenuation spectra for a 110 nm wide nanoribbon array with different PMMA overlayer thicknesses are shown in Figure 5a. Here, it is observed that the plasmon resonance strongly red-shifts with increasing PMMA layer thickness and that the shift saturates for PMMA layer thicknesses larger than about 20 nm. The decrease in the plasmon resonance frequency with an increase in the dielectric constant from the surrounding environment is a well-known

dx.doi.org/10.1021/nl404824w | Nano Lett. 2014, 14, 1573−1577

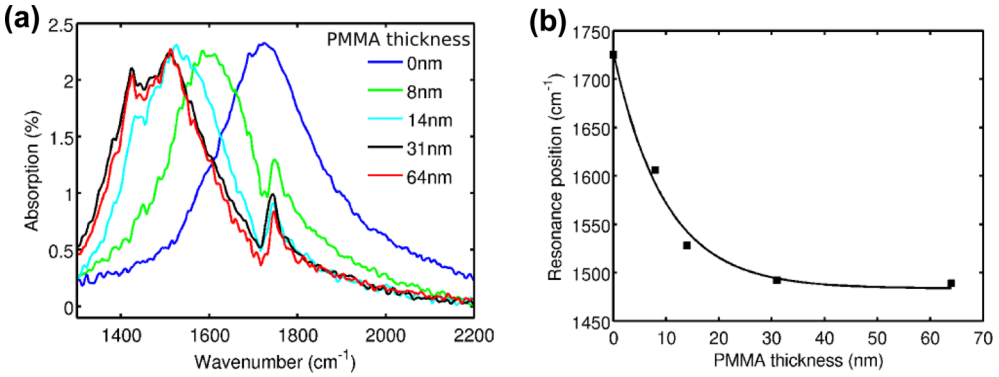

Figure 5. (a) Graphene plasmon transmission attenuation spectra for different PMMA film thicknesses ranging from 0 to 64 nm. Along with the C=O stretch, the enhancement of another vibration (O−CH_3 bending) at about 1450 cm^{-1} becomes apparent at the higher thicknesses. Note that the PMMA induced detuning of the two modes from the plasmon frequency is opposite. (b) The dependence of the plasmon resonance position on the thickness of the PMMA layer. The exponential fit (black line) gives a plasmon field decay length in PMMA of 10 ± 2 nm.

behavior of plasmons in metal nanostructures.[26] The observed ∼260 cm^{-1} shift of the resonance frequency from bare ribbons to the 64 nm overlayer corresponds to a 15% decrease in the resonance frequency. In the limit of a thick overlayer, the plasmon field above the graphene surface would be completely confined within the PMMA. An intuitive understanding of this red-shift can be gained by considering the dispersion relation of unpatterned graphene.[17] In this case, the dielectric screening of the plasmon field will result in a reduction of the resonance frequency by 18% (see Supporting Information for details),[17] comparable to the measured result for the nanoribbon array. The ∼260 cm^{-1} red-shift of the graphene plasmon peak can therefore be understood in terms of dielectric screening from the environment. This shift corresponds to a refractive index sensitivity of ∼2650 nm/RIU, a figure of merit used in the plasmon sensor community.[27−29] More importantly, saturation of the red-shift gives a direct estimation of the plasmon field decay length into the dielectric. This saturation can be fitted to the exponential function $f = f_0 - \Delta f \exp(-d/d_0)$, where f is the resonance frequency in the limit of a very thick PMMA layer, Δf is the maximum (negative) frequency shift, and d_0 is the decay length. From the fitting, we obtain a field decay length of $d_0 = 10 \pm 2$ nm (Figure 5b). Considering that the incident light wavelength is $\lambda_0 \sim 6$ μm, this decay length corresponds to a confinement factor in the normal direction of $\lambda_0/2\pi d_0 \sim 100$. This very short decay length indicates that graphene plasmonics could be a good candidate for surface sensing applications in the infrared and far-infrared regions.

To demonstrate the specificity of the enhanced light-matter interaction, PVP was also studied. Height and phase-contrast AFM analysis of the PVP-coated nanoribbon array reveals that the maximum thickness of the PVP film is 3 nm. Figure 6 shows the spectrum of graphene nanoribbons covered by this overlayer. Similar to the PMMA case, a phonon induced transparency valley appears within the plasmon resonance peak. Detection of this feature in such a thin and nonuniform film further demonstrates the plasmon-induced enhancement capability of the nanoribbon array. Moreover, due to the 50 cm^{-1} difference in the carbonyl double-bond vibrational peak frequencies of PMMA and PVP, the locations of the corresponding transparency valleys also differ by the same amount. This demonstrates the molecular specificity of this sensing technology, even without surface functionalization.

In conclusion, we have demonstrated graphene plasmon enhanced vibrational sensing of surface-adsorbed polymers.

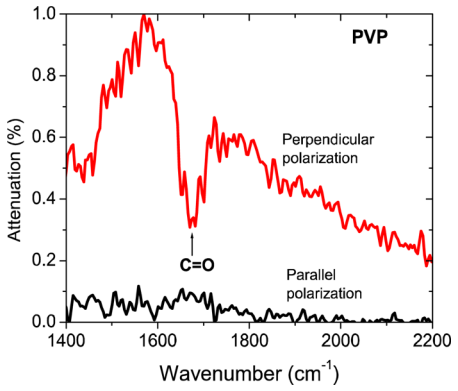

Figure 6. Attenuation spectra for graphene nanoribbons covered with a PVP layer with a thickness <3 nm, for perpendicular (red line) and parallel (black line) polarizations.

The detection sensitivity increases by a factor of about 5, as evident from the height of the induced transparency in the IR attenuation spectra of the coupled plasmon-vibrational mode system. The modulation of the graphene plasmon attenuation spectrum by surface-adsorbed polymers is due to near-field electromagnetic coupling, as supported by FDTD simulations and a phenomenological coupled oscillator model. The large magnitude of this modulation as compared to the absorption of the polymer film is caused by a strong enhancement in the near-field intensity. Furthermore, this plasmonic enhancement is confined to the vicinity of the surface, as the plasmon field decay length is measured to be ∼10 nm. Lastly, this vibration sensing technique exhibits molecular specificity; that is, different molecular compounds can be differentiated from the peak frequencies of the vibrational mode induced transparencies.

■ ASSOCIATED CONTENT

Supporting Information

FDTD simulation and dielectric screening details. This material is available free of charge via the Internet at http://pubs.acs.org.

■ AUTHOR INFORMATION

Corresponding Author

*E-mail: avouris@us.ibm.com.

Notes

The authors declare no competing financial interest.

■ ACKNOWLEDGMENTS

The authors would like to acknowledge valuable discussions with Dr. Tony Low. The FDTD simulations were performed via the computer cluster in the Center for Functional Nanomaterials (CFN) at the Brookhaven National Laboratory (BNL), which is supported by the U.S. Department of Energy, Office of Basic Energy Sciences, under Contract No. DE-AC02-98CH10886. Support for modeling studies at Columbia University was provided in part from the National Science Foundation through grant DMR-1106225 and from the Office of Naval Research.

■ REFERENCES

(1) Novoselov, K. S.; Geim, A. K.; Morozov, S. V.; Jiang, D.; Katsnelson, M. I.; Grigorieva, I. V.; Dubonos, S. V.; Firsov, A. A. *Nature* **2005**, *438*, 197−200.
(2) Zhang, Y.; Tan, Y.-W.; Stormer, H. L.; Kim, P. *Nature* **2005**, *438*, 201−204.
(3) Geim, A. K.; Novoselov, K. S. *Nat. Mater.* **2007**, *6*, 183−191.
(4) Ju, L.; Geng, B.; Horng, J.; Girit, C.; Martin, M.; Hao, Z.; Bechtel, H. A.; Liang, X.; Zettl, A.; Shen, Y. R.; Wang, F. *Nat. Nanotechnol.* **2011**, *6*, 630−634.
(5) Fei, Z.; Rodin, A. S.; Andreev, G. O.; Bao, W.; McLeod, A. S.; Wagner, M.; Zhang, L. M.; Zhao, Z.; Thiemens, M.; Dominguez, G.; Fogler, M. M.; Neto, A. H. C.; Lau, C. N.; Keilmann, F.; Basov, D. N. *Nature* **2012**, *487*, 82−85.
(6) Chen, J.; Badioli, M.; Alonso-Gonzalez, P.; Thongrattanasiri, S.; Huth, F.; Osmond, J.; Spasenovic, M.; Centeno, A.; Pesquera, A.; Godignon, P.; Zurutuza Elorza, A.; Camara, N.; de Abajo, F. J. G.; Hillenbrand, R.; Koppens, F. H. L. *Nature* **2012**, *487*, 77−81.
(7) Koppens, F. H. L.; Chang, D. E.; García de Abajo, F. J. *Nano Lett.* **2011**, *11*, 3370−3377.
(8) Fei, Z.; Andreev, G. O.; Bao, W.; Zhang, L. M.; S. McLeod, A.; Wang, C.; Stewart, M. K.; Zhao, Z.; Dominguez, G.; Thiemens, M.; Fogler, M. M.; Tauber, M. J.; Castro-Neto, A. H.; Lau, C. N.; Keilmann, F.; Basov, D. N. *Nano Lett.* **2011**, *11*, 4701−4705.
(9) Yan, H.; Low, T.; Zhu, W.; Wu, Y.; Freitag, M.; Li, X.; Guinea, F.; Avouris, P.; Xia, F. *Nat. Photonics* **2013**, *7*, 394−399.
(10) Yan, H.; Low, T.; Guinea, F.; Xia, F.; Avouris, P. *arXiv:1310.4394v1* **2013**.
(11) Liu, F.; Cubukcu, E. *Phys. Rev. B* **2013**, *88*, 115439.
(12) Luk'yanchuk, B.; Zheludev, N. I.; Maier, S. A.; Halas, N. J.; Nordlander, P.; Giessen, H.; Chong, C. T. *Nat. Mater.* **2010**, *9*, 707−715.
(13) Adato, R.; Yanik, A. A.; Amsden, J. J.; Kaplan, D. L.; Omenetto, F. G.; Hong, M. K.; Erramilli, S.; Altug, H. *Proc. Natl. Acad. Sci.* **2009**, *106*, 19227−19232.
(14) Neubrech, F.; Pucci, A.; Cornelius, T. W.; Karim, S.; García-Etxarri, A.; Aizpurua, J. *Phys. Rev. Lett.* **2008**, *101*, 157403.
(15) Halas, N. J.; Lal, S.; Chang, W.-S.; Link, S.; Nordlander, P. *Chem. Rev.* **2011**, *111*, 3913−3961.
(16) Horng, J.; Chen, C.-F.; Geng, B.; Girit, C.; Zhang, Y.; Hao, Z.; Bechtel, H. A.; Martin, M.; Zettl, A.; Crommie, M. F.; Shen, Y. R.; Wang, F. *Phys. Rev. B* **2011**, *83*, 165113.
(17) Jablan, M.; Buljan, H.; Soljačić, M. *Phys. Rev. B* **2009**, *80*, 245435.
(18) Hwang, E. H.; Das Sarma, S. *Phys. Rev. B* **2007**, *75*, 205418.
(19) Yan, H.; Li, X.; Chandra, B.; Tulevski, G.; Wu, Y.; Freitag, M.; Zhu, W.; Avouris, P.; Xia, F. *Nat. Nanotechnol.* **2012**, *7*, 330−334.
(20) Freitag, M.; Low, T.; Zhu, W.; Yan, H.; Xia, F.; Avouris, P. *Nat. Commun.* **2013**, *4*, 1951.
(21) Harris, S. E. *Phys. Today* **1997**, *50*, 36−42.
(22) Weis, S.; Riviere, R.; Deleglise, S.; Gavartin, E.; Arcizet, O.; Schliesser, A.; Kippenberg, T. J. *Science* **2010**, *330*, 1520−1523.
(23) Alzar, C. L. G.; Martinez, M. A. G.; Nussenzveig, P. *Am. J. Phys.* **2002**, *70*, 37−41.
(24) Low, T.; Guinea, F.; Yan, H.; Xia, F.; Avouris, P. *arXiv:1310.4693* **2013**.
(25) Tinkham, M. *Phys. Rev.* **1956**, *104*, 845−846.
(26) Wang, F.; Shen, Y. R. *Phys. Rev. Lett.* **2006**, *97*, 206806.
(27) Homola, J.; Yee, S. S.; Gauglitz, G. *Sens. Actuators, B* **1999**, *54*, 3−15.
(28) Liedberg, B.; Nylander, C.; Lunström, I. *Sens. Actuators* **1983**, *4*, 299−304.
(29) Zhao, Y.; Hu, X.; Chen, G.; Zhang, X.; Tan, Z.; Chen, J.; Ruoff, R. S.; Zhu, Y.; Lu, Y. *Phys. Chem. Chem. Phys.* **2013**, *15*, 17118−17125.